Nanoscale

COMMUNICATION

View Article Online
View Journal | View Issue

Cite this: *Nanoscale*, 2016, **8**, 16172

Received 20th May 2016,
Accepted 18th August 2016

DOI: 10.1039/c6nr04103e

www.rsc.org/nanoscale

Direct real-time detection of single proteins using silicon nanowire-based electrical circuits†

Jie Li,[a,b] Gen He,[a,b] Hiroshi Ueno,[c] Chuancheng Jia,[b] Hiroyuki Noji,*[c] Chuanmin Qi*[a] and Xuefeng Guo*[b,d]

We present an efficient strategy through surface functionalization to build a single silicon nanowire field-effect transistor-based biosensor that is capable of directly detecting protein adsorption/desorption at the single-event level. The step-wise signals in real-time detection of His-tag F_1-ATPases demonstrate a promising electrical biosensing approach with single-molecule sensitivity, thus opening up new opportunities for studying single-molecule biophysics in broad biological systems.

The development of efficient approaches to detect chemical and biological species in a nondestructive manner with high sensitivity, with the ultimate aim of single-molecule/single-event sensitivity, is of great importance to many applications ranging from clinical diagnostics and environment preservation to national defense and bioterrorism prevention.[1–5] In this regard, discrete nanoscale electrical chemo-/bio-sensor platforms have been successfully developed by using different nanomaterials or nanostructures as sensing elements, including carbon nanotubes/graphene,[6–10] nanowires,[11–14] nanopores,[15–17] nanoclusters,[18,19] and molecular junctions.[20–22]

In this study, we describe another efficient approach to build nanoscale electrical biosensors (Fig. 1) that are able to directly detect individual motor proteins through the combination of microfabrication and directed self-assembly by using silicon nanowires (SiNWs) as local electrical probes. Because negatively-charged proteins under certain pH buffers act as a local gate after assembly and electrostatically modulate the carrier intensity inside the nanowires, these specific adsorption/desorption processes can be distinguished one by one at an ultra-low concentration. One-dimensional SiNWs, whose conductance is strongly dependent on the local charge density, are one of the most attractive semiconductor nanomaterials with remarkable properties, such as excellent biocompatibility, superior electrical properties, precise controllability, flexible surface tailorability and good size comparability. These properties set the foundation for making new types of high-gain SiNW field-effect transistor (FET)-based biosensors for broad applications in biological and life sciences. At present, SiNW FETs have been used for DNA detection, chemical/virus diagnosis and special gas detection.[23–34] We chose an ATP-driven rotary motor protein F_1-ATPase (F_1-$\alpha_3\beta_3\gamma$(α(His_6-N-terminus/C193S)β(His_{10}-Lys_7-N-terminus)γ(S107C/I210C)), expressed in thermophilic *bacillus* PS3[35]) as the detection target because F_1, as a part of ATP synthase that is one of the most responsible enzymes for ATP homeostasis, is a representative molecular machine that interconverts the chemical energy of ATP and mechanical energy with high efficiency. Thereby, F_1 has crucial roles in cellular bioenergetics and physiological activities.[36–40] Another motivation to target F_1 is that the size of F_1,

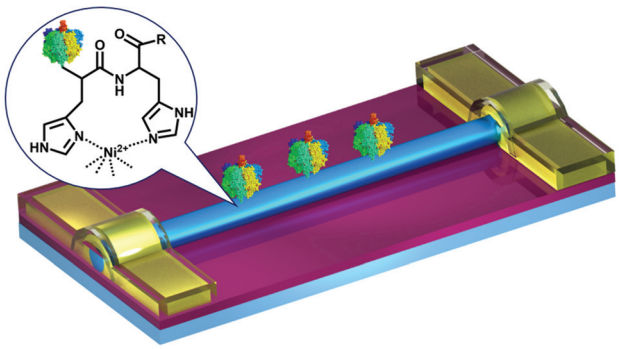

Fig. 1 Schematic demonstration of SiNW FET-based electrical biosensors, where Au electrodes are passivated by using a thermally deposited 50 nm-thick SiO_2 layer. The inset shows how His-tag F_1-ATPase is immobilized on the surface of SiNWs through Ni^{2+} chelation.

[a]*Key Laboratory of Radiopharmaceuticals, Ministry of Education, College of Chemistry, Beijing Normal University, Beijing 100875, P. R. China. E-mail: qichuanmin@bnu.edu.cn*
[b]*Beijing National Laboratory for Molecular Sciences, State Key Laboratory for Structural Chemistry of Unstable and Stable Species, College of Chemistry and Molecular Engineering, Peking University, Beijing 100871, P. R. China. E-mail: guoxf@pku.edu.cn*
[c]*Department of Applied Chemistry, School of Engineering, The University of Tokyo, Tokyo 113-8654, Japan. E-mail: hnoji@appchem.t.u-tokyo.ac.jp*
[d]*Department of Materials Science and Engineering, College of Engineering, Peking University, Beijing 100871, P. R. China*

†Electronic supplementary information (ESI) available. See DOI: 10.1039/c6nr04103e

~10 nm outer diameter, is almost compatible with SiNWs. Interestingly, by programmably integrating specific recognition groups into SiNW FET-based electrical circuits, we realized direct real-time monitoring of the adsorption/desorption processes of proteins at the single-event level in combination with microfluidics, thus offering a novel route to carry out future single-molecule detection or dynamics studies in biological systems.

In general, the strategy used for SiNW FET modification is to functionalize the whole device surface with aminosilanes after device fabrication.[26,41] The competitive adsorption from functional group-modified substrates significantly reduces the detection sensitivity. To confine detection targets to be specifically adsorbed on the surface of SiNWs and increase the sensitivity (Fig. 1), we developed a new processing strategy to avoid surface modification of the substrate as described in Fig. 2. Firstly, we treated high-quality pristine SiNWs (ESI, Fig. S1†), which were grown on silicon substrates by a standard Au-catalysed vapor–liquid–solid (VLS) method,[2] with an aminosilane gas (3-(2-aminoethylamino)propyltrimethoxysilane (N-APTMS)) (Sigma-Aldrich, 99%) in a vacuum desiccator for several hours before transfer, thus forming amino SiNWs. This operation also retained the original upright growth morphology of SiNWs so that they could be easily transferred to the clean doped silicon wafers with *circa* 1000 nm of thermally grown SiO_2 on the surface and well-aligned by mechano-sliding.[42]

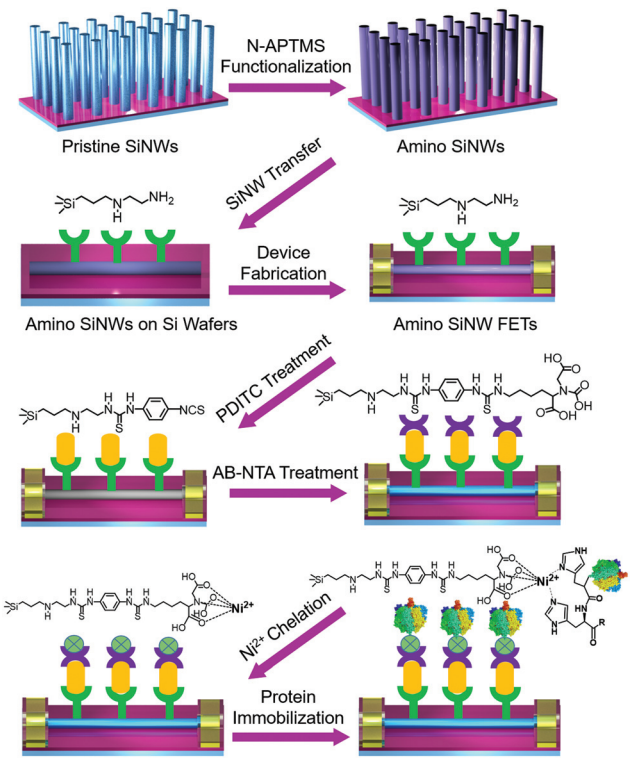

Fig. 2 A depiction of the programmed strategy developed for building SiNW FET-based electrical biosensors to measure the absorption/desorption processes of proteins at the single-event level. Different colours of silicon nanowires represent different stages of surface modification.

By using photolithography, high-density SiNW FET arrays were then made on silicon substrates (ESI, Fig. S2†) (details of the device fabrication can be found in the ESI†). To rule out potential artifacts from the Schottky barrier modification between the analytes and Au electrodes, we passivated Au leads by employing a 50 nm-thick layer of silicon oxide through electron beam thermal evaporation after electrode deposition. This process left the free amino groups only on the surface of SiNWs available for subsequent modification. Note that the similarity of transfer curves before and after the photolithographical patterning and e-beam thermal deposition process shown in Fig. S3A† demonstrates the almost non-disturbing effect of the fabrication process on the properties of SiNWs.

After device fabrication, we performed the sequential chemical reactions of functionalized devices with phenylene-1,4-diisothiocyanate (PDICT, Sigma-Aldrich 99%), Nα,Nα-bis (carboxymethyl)-L-lysine hydrate (AB-NTA, Sigma-Aldrich 97%) and $NiCl_2$ (Sigma-Aldrich, 99.99%), respectively, which only occurred on the aminated surface of SiNWs (Fig. 2). To prove the effectiveness of surface functionalization, we characterized each step on silicon wafers with the bare SiO_2 surface by using X-ray photoelectron spectroscopy (XPS) and Fourier transform infrared spectroscopy (FTIR). After silanization with N-APTMS, in comparison with the bare SiO_2 surface (ESI, Fig. S4A†), there is a clear indication of the emergence of the N 1s peak due to the attachment of N-APTMS (Fig. 3A). The high-resolution N 1s peak consists of two well-separated components centered at ~398.9 eV and ~399.9 eV (Fig. 3B), which should be attributed to nitrogen atoms in $-NH_2$ and –NH–,[43,44] respectively. The successful attachment of N-APTMS was further confirmed by the FTIR spectrum where we observed the new N–H stretch at ~3300 cm^{-1} (Fig. 3A inset).[43] After further reaction with PDITC, we found the appearance of a new S 2s peak (Fig. 3C), which only possibly originated from the PDITC component. The high-resolution S 2s core level is split into two components at ~226.5 eV and ~230.9 eV (ESI, Fig. S4C†), which are characteristic of the sulphur atoms in the thiourea unit formed from the surface reaction and –NCS group, respectively.[44,45] In addition to this, the N 1s peak shows the loss of the nitrogen atom of $-NH_2$ at ~398.9 eV and the appearance of the nitrogen atom of –N = (~401.8 eV) (Fig. 3D). Note that the main peak at ~400.0 eV should be attributed to nitrogen atoms from both –NH– and thiourea groups. These results consistently provide unambiguous evidence that PDITC was immobilized on the surface of SiNWs. Although the reaction between AB-NTA and PDITC didn't introduce new elements (ESI, Fig. S4†), we did observe the disappearance of the sulphur atom of –NCS in the S 2s core level due to the symmetric thiourea formation (ESI, Fig. S4D†). Further important evidence for the whole procedure is the gradual changes in the elemental ratios of C : N : S. The summary of the changes in elemental ratios from XPS along with the process is listed in Table S1.† These values are in good agreement with theoretical calculation, thus again proving the success of the whole strategy developed here. More details of the XPS analysis can be found in the ESI.† After further Ni^{2+} chelation to form

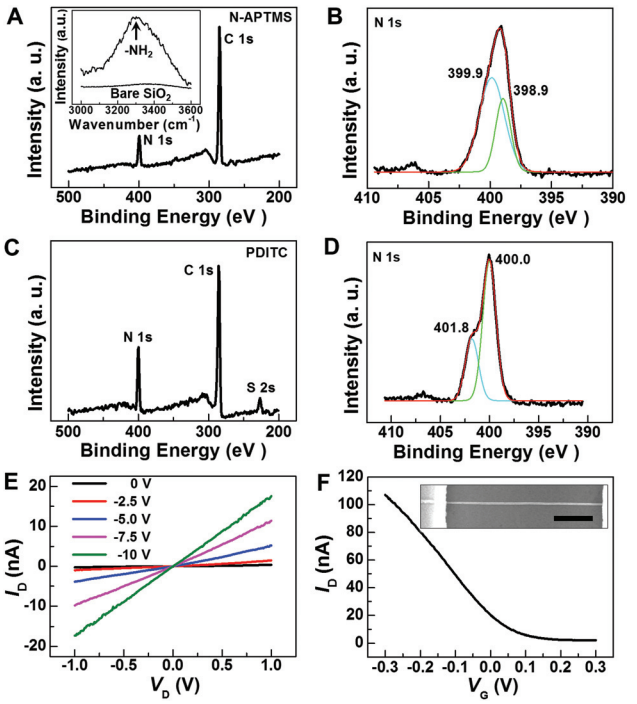

Fig. 3 Spectral and electrical characterization. (A) XPS spectrum after N-APTMS attachment. The inset shows the FTIR spectrum of amine groups. (B) High-resolution N 1s core level spectrum after N-APTMS attachment. (C) XPS spectrum after further PDITC treatment. (D) High-resolution N 1s core level spectrum after further PDITC treatment. (E) Output characteristics of a p-type SiNW FET under a global backgate. (F) Transfer characteristics under a liquid gate of the same device. V_D = 0.1 V. The inset shows the SEM image of the device. The scale bar is 1 μm.

functional Ni-NTA end groups (Fig. 2), the resultant devices were ready for the following biodetection. Note that this highly selective chemical modification procedure limits the following bio-recognition events to take place on the surface of SiNWs (not on silicon substrates) (ESI, Fig. S5†), thus almost precluding the competitive capacity of protein immobilization on the substrate and correspondingly ensuring successful detection in solutions with an ultralow concentration. In fact, only a few strategies have been developed to achieve both high sensitivity and selectivity, such as oxidation of carbon nanotubes to form surface defects[46,47] and empirical buffer washing to remove excess binding proteins through noncovalent π–π stacking with carbon nanotubes.[48–50] However, these methods meet the difficulties of low device fabrication yield and poor controllability.

Before biodetection, we measured the electrical properties of SiNW FETs after multi-step modification. As shown in Fig. 3E and F, the initial electrical characterization demonstrated that SiNWs show typical p-type properties with good ohmic contacts. The inset in Fig. 3F shows an individual SiNW that nicely spans between the metal electrodes with a *circa* 4 μm space. Note that the device was turned on at nearby 0 V under liquid gate modulation (with the sensitivity of ~800 nA V^{-1} and the subthreshold swing of ~100 mV dec^{-1}, Fig. S3B and S3C†). This is the subthreshold region of SiNW FETs where they possess the highest sensitivity.[51] Any tiny changes in environmental charges produced by charged protein attachment could induce an additional gate that efficiently modulates the conductance of SiNW FET-based biosensors. The diameter of SiNWs used in this study varies in the range of 20–40 nm.

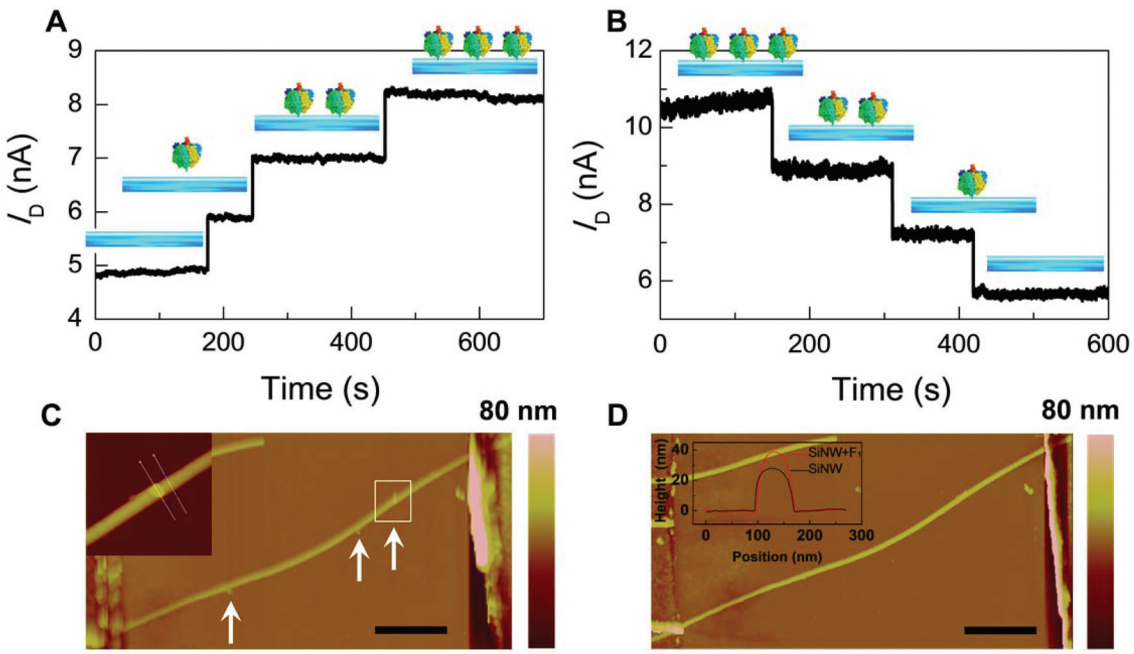

Fig. 4 Sensing properties. (A, B) Real-time recordings of the absorption/desorption processes of F_1-ATPases, showing the gradual changes in I_D with three steps. V_D = 0.1 V and V_G = 0 V. (C, D) Corresponding AFM images after protein delivery (C, inset shows an enlarged image of a single F_1 protein) and after further EDTA treatment (D, inset is the height profile of the bare silicon nanowire and the nanowire with an adsorbed F_1 protein particle in (C) inset. The total height of F_1 is ~12 nm including a ~2 nm linkage). The scale bar is 1 um.

After Ni^{2+} chelation and electrical characterization, we then turned our attention to studying their biosensing properties. In combination with microfluidics (ESI, Fig. S6†), we realized real-time, direct detection of the binding/unbinding processes of motor proteins through high-yield reversible chelation between Ni-NTA and the imidazole of His-tags in F_1-ATPases at the single-event level (Fig. 1 and 2). Before delivering proteins to the device, a pure tris-buffer solution (10 mM tris-HCl, 27.6 mM NaCl, 0.54 mM KCl, pH = 8.0, Sigma-Aldrich) was introduced to stabilize the device for about 100 s (ESI, Fig. S7†). As shown in Fig. 4A, remarkably we observed the gradual increases in the source–drain current (I_D) in three steps while the buffer solution containing the negatively-charged protein particles (~1.84 nM) was flowed through the functionalized surface of p-type SiNWs. This is reasonable because the one-by-one adsorption of motor proteins introduces negative charges (pH = 8.0) on the SiNW surface that function as an additional gate to increase the density of hole carriers in the conductive channel (and thus the device conductance) (ESI, Fig. S8†). This process is reversible since we captured the step-by-step, opposite current decreases upon exposure to the solution of EDTA (1 mM, pH = 8.00, Sigma-Aldrich), which has stronger coordinating ability with Ni^{2+} than imidazoles of His-tags to desorb proteins one-by-one from the surface of SiNWs (Fig. 4B).

To confirm whether the step-wise signals really originated from F_1 adsorption/desorption, we scanned the device by using atomic force microscopy (AFM) to count the number of F_1-ATPases on the SiNW surface immediately after real-time measurements. The AFM image in Fig. 4C shows the surface morphology of the same device used in Fig. 4A. It is clear that the total number of individual F_1-ATPase particles (~10 nm, Fig. 4C inset and Fig. 4D inset) found on the SiNW surface is 3, which is exactly in agreement with the step numbers observed in electrical measurements (Fig. 4A). Furthermore, as shown in Fig. 4D, we did not find any proteins on the SiNW surface after further EDTA treatments. These results surely confirm the capability of our strategy for direct real-time detection of biological species with single-molecule/single-event sensitivity. To demonstrate the reproducibility of this detection platform, we carried out additional electrical measurements of the reversible adsorption/desorption processes of proteins with four separate events as shown in Fig. S9 in the ESI.† The AFM characterization in Fig. S9C and S9D† also proves the presence of four individual proteins, thus confirming these step-by-step processes.

Conclusions

In conclusion, we present herein a reliable electrical detection platform that is able to achieve direct, real-time measurement of proteins with single-molecule sensitivity through the combination of sophisticated microfabrication and programmed self-assembly by using high-gain SiNWs as local sensing elements. As the verification of the number of detection targets before testing is crucial to confirm the reliable signal source and the data analysis for biomolecular dynamics research, the unfavourable statistics of feedback controlled oxidation,[52] poor control of the target and low binding yield of noncovalent assembly methods[49] are undesirable for this goal. Our nondestructive label-free electrical detection method nicely integrates the target recognition, number verification and real-time monitoring, which is significant to further applications. On the other hand, in comparison with the optical methods, this label-free electrical detection is a good compensation with obvious advantages, such as being without fluorescent labelling and bleaching problems. Therefore, this platform can be naturally extended to detect many other charged chemical and biological species for broad applications, such as clinic diagnostics, environment preservation, national defense, and bioterrorism prevention. In addition to these, this methodology also opens up an effective and immediate route to study fast single-molecule/single-event dynamics in an interdisciplinary realm, for example genic polymorphism, protein folding, and enzymatic activity.

Acknowledgements

We acknowledge primary financial support from NSFC (21225311, 91333102, 21373014, and 21571021) and the 973 Project (2012CB921404).

References

1 N. L. Rosi and C. A. Mirkin, *Chem. Rev.*, 2005, **105**, 1547.
2 F. Patolsky, G. Zheng and C. M. Lieber, *Nat. Protoc.*, 2006, **1**, 1711.
3 J. Liu, Z. Cao and Y. Lu, *Chem. Rev.*, 2009, **109**, 1948.
4 D. R. Kauffman and A. Star, *Chem. Soc. Rev.*, 2008, **37**, 1197.
5 X. Xie, W. Xu and X. Liu, *Acc. Chem. Res.*, 2012, **45**, 1511.
6 B. L. Allen, P. D. Kichambare and A. Star, *Adv. Mater.*, 2007, **19**, 1439.
7 G. Gruner, *Anal. Biochem.*, 2006, **384**, 322.
8 S. Liu, Q. Shen, Y. Cao, L. Gan, Z. Wang, M. L. Steigerwald and X. Guo, *Coord. Chem. Rev.*, 2010, **254**, 1101.
9 W. Yang, K. R. Ratinac, S. P. Ringer, P. Thordarson, J. J. Gooding and F. Braet, *Angew. Chem., Int. Ed.*, 2010, **49**, 2114.
10 S. Liu and X. Guo, *NPG Asia Mater.*, 2012, **4**, e23.
11 K.-I. Chen, B.-R. Li and Y.-T. Chen, *Nano Today*, 2011, **6**, 131.
12 A. Mulchandani and N. V. Myung, *Curr. Opin. Biotechnol.*, 2011, **22**, 502.
13 F. Patolsky, G. Zheng and C. M. Lieber, *Anal. Chem.*, 2006, **78**, 4260.
14 G. He, J. Li, H. Ci, C. Qi and X. Guo, *Angew. Chem., Int. Ed.*, 2016, **55**, 9036.
15 S. Howorka and Z. Siwy, *Chem. Soc. Rev.*, 2009, **38**, 2360.

16 H. Bayley and L. Jayasinghe, *Mol. Membr. Biol.*, 2004, **21**, 209.
17 H. Bayley and P. S. Cremer, *Nature*, 2001, **413**, 226.
18 L. Soleymani, Z. Fang, E. H. Sargent and S. O. Kelley, *Nat. Nanotechnol.*, 2009, **4**, 844.
19 X. Chen, Z. Guo, G.-M. Yang, J. Li, M.-Q. Li, J.-H. Liu and X.-J. Huang, *Mater. Today*, 2010, **13**, 28.
20 X. Guo, *Adv. Mater.*, 2013, **25**, 3397.
21 C. Jia, B. Ma, N. Xin and X. Guo, *Acc. Chem. Res.*, 2015, **48**, 2565.
22 Y. Zhao, B. Ashcroft, P. Zhang, H. Liu, S. Sen, W. Song, J. Im, B. Gyarfas, S. Manna, S. Biswas, C. Borges and S. Lindsay, *Nat. Nanotechnol.*, 2014, **9**, 466.
23 X. Duan, R. Gao, P. Xie, T. Cohen-Karni, Q. Qing, H. S. Choe, B. Tian, X. Jiang and C. M. Lieber, *Nat. Nanotechnol.*, 2012, **7**, 174.
24 B. Tian, T. Cohen-Karni, Q. Qing, X. Duan, P. Xie and C. M. Lieber, *Science*, 2010, **329**, 830.
25 E. Stern, J. F. Klemic, D. A. Routenberg, P. N. Wyrembak, D. B. Turner-Evans, A. D. Hamilton, D. A. LaVan, T. M. Fahmy and M. A. Reed, *Nature*, 2007, **445**, 519.
26 Y. Cui, Q. Wei, H. Park and C. M. Lieber, *Science*, 2001, **293**, 1289.
27 F. Shen, J. Wang, Z. Xu, Y. Wu, Q. Chen, X. Li, X. Jie, L. Li, M. Yao, X. Guo and T. Zhu, *Nano Lett.*, 2012, **12**, 3722.
28 F. Shen, M. Tan, Z. Wang, M. Yao, Z. Xu, Y. Wu, J. Wang, X. Guo and T. Zhu, *Environ. Sci. Technol.*, 2011, **45**, 7473.
29 T. W. Lin, P. J. Hsieh, C. L. Lin, Y. Y. Fang, J. X. Yang, C. C. Tsai, P. L. Chiang, C. Y. Pan and Y. T. Chen, *Proc. Natl. Acad. Sci. U. S. A.*, 2010, **107**, 1047.
30 J. D. Wulfkuhle, L. A. Liotta and E. F. Petricoin, *Nat. Rev. Cancer*, 2003, **3**, 267.
31 R. Etzioni, N. Urban, S. Ramsey, M. McIntosh, S. Schwartz, B. Reid, J. Radich, G. Anderson and L. Hartwell, *Nat. Rev. Cancer*, 2003, **3**, 243.
32 D. Sidransky, *Nat. Rev. Cancer*, 2002, **2**, 210.
33 F. X. Shen, J. D. Wang, Z. Q. Xu, Y. Wu, Q. Chen, X. G. Li, X. Jie, L. D. Li, M. S. Yao, X. F. Guo and T. Zhu, *Nano Lett.*, 2012, **12**, 3722.
34 F. Patolsky, G. F. Zheng, O. Hayden, M. Lakadamyali, X. W. Zhuang and C. M. Lieber, *Proc. Natl. Acad. Sci. U. S. A.*, 2004, **101**, 14017.
35 S. Furuike, K. Adachi, N. Sakaki, R. Shimo-Kon, H. Itoh, E. Muneyuki, M. Yoshida and K. Kinosita Jr., *Biophys. J.*, 2008, **95**, 761.
36 H. Noji, R. Yasuda, M. Yoshida and K. Kinosita, *Nature*, 1997, **386**, 299.
37 H. Itoh, A. Takahashi, K. Adachi, H. Noji, R. Yasuda, M. Yoshida and K. Kinosita, *Nature*, 2004, **427**, 465.
38 H. Ueno, T. Suzuki, K. Kinosita and M. Yoshida, *Proc. Natl. Acad. Sci. U. S. A.*, 2005, **102**, 1333.
39 K. Adachi, K. Oiwa, T. Nishizaka, S. Furuike, H. Noji, H. Itoh, M. Yoshida and K. Kinosita Jr., *Cell*, 2007, **130**, 309.
40 T. Uchihashi, R. Iino, T. Ando and H. Noji, *Science*, 2011, **333**, 755.
41 Y. Engel, R. Elnathan, A. Pevzner, G. Davidi, E. Flaxer and F. Patolsky, *Angew. Chem., Int. Ed.*, 2010, **49**, 6830.
42 J. Yao, H. Yan and C. M. Lieber, *Nat. Nanotechnol.*, 2013, **8**, 329.
43 A. Danon, P. C. Stair and E. Weitz, *J. Phys. Chem. C*, 2011, **115**, 11540.
44 H. A. Bullen, M. J. Dorko, J. K. Oman and S. J. Garrett, *Surf. Sci.*, 2003, **531**, 319.
45 D. K. Bhowmick, S. Linden, A. Devaux, L. De Cola and H. Zacharias, *Small*, 2012, **8**, 592.
46 S. Sorgenfrei, C.-y. Chiu, R. L. Gonzalez Jr., Y.-J. Yu, P. Kim, C. Nuckolls and K. L. Shepard, *Nat. Nanotechnol.*, 2011, **6**, 126.
47 S. Sorgenfrei, C.-y. Chiu, M. Johnston, C. Nuckolls and K. L. Shepard, *Nano Lett.*, 2011, **11**, 3739.
48 Y. K. Choi, I. S. Moody, P. C. Sims, S. R. Hunt, B. L. Corso, I. Perez, G. A. Weiss and P. G. Collins, *Science*, 2012, **335**, 319.
49 T. J. Olsen, Y. Choi, P. C. Sims, O. T. Gul, B. L. Corso, C. Dong, W. A. Brown, P. G. Collins and G. A. Weiss, *J. Am. Chem. Soc.*, 2013, **135**, 7855.
50 P. C. Sims, I. S. Moody, Y. Choi, C. Dong, M. Iftikhar, B. L. Corso, O. T. Gul, P. G. Collins and G. A. Weiss, *J. Am. Chem. Soc.*, 2013, **135**, 7861.
51 X. P. A. Gao, G. Zheng and C. M. Lieber, *Nano Lett.*, 2009, **10**, 547.
52 S. Sorgenfrei, C.-y. Chiu, R. L. Gonzalez, Y.-J. Yu, P. Kim, C. Nuckolls and K. L. Shepard, *Nat. Nanotechnol.*, 2011, **6**, 126.